

Phonon anharmonicity in thermoelectric palladium sulfide by Raman spectroscopy

Liu-Cheng Chen, Zi-Yu Cao, Hao Yu, Bin-Bin Jiang, Lei Su, Xun Shi, Li-Dong Chen, and Xiao-Jia Chen

Citation: *Appl. Phys. Lett.* **113**, 022105 (2018); doi: 10.1063/1.5041973

View online: <https://doi.org/10.1063/1.5041973>

View Table of Contents: <http://aip.scitation.org/toc/apl/113/2>

Published by the [American Institute of Physics](#)

Articles you may be interested in

[Graphdiyne under pressure: A Raman study](#)

Applied Physics Letters **113**, 021901 (2018); 10.1063/1.5023619

[Mid-wavelength high operating temperature barrier infrared detector and focal plane array](#)

Applied Physics Letters **113**, 021101 (2018); 10.1063/1.5033338

[Bandgap opening in hydrogenated germanene](#)

Applied Physics Letters **112**, 171607 (2018); 10.1063/1.5026745

[Thermal tuning of silicon terahertz whispering-gallery mode resonators](#)

Applied Physics Letters **113**, 011101 (2018); 10.1063/1.5036539

[Interdot spin transfer dynamics in laterally coupled excited spin ensemble of high-density InGaAs quantum dots](#)

Applied Physics Letters **113**, 023104 (2018); 10.1063/1.5022641

[A non-collinear double MgO based perpendicular magnetic tunnel junction](#)

Applied Physics Letters **113**, 022403 (2018); 10.1063/1.5038060

Quantum Design Brings You the Next Generation Magneto-Optic Cryostat



Only be limited by your imagination...

Room Temperature Window
Split-Coil Conical Magnet
Sample Pod
User Wiring Ports

Learn More

Quantum Design
qdusa.com/opticool5

8 Optical Access Ports: 7 Side; 1 Top
Temperature Range: 1.7 K to 350 K
7 T Split-Coil Conical Magnet
Low Vibration: <10 nm peak-to-peak
89 mm x 84 mm Sample Volume
Automated Temperature & Magnet Control
Cryogen Free

Phonon anharmonicity in thermoelectric palladium sulfide by Raman spectroscopy

 HPSTAR
 601-2018

 Liu-Cheng Chen,^{1,2,3} Zi-Yu Cao,³ Hao Yu,³ Bin-Bin Jiang,^{4,5} Lei Su,⁶ Xun Shi,⁴
 Li-Dong Chen,⁴ and Xiao-Jia Chen^{3,a)}
¹Key Laboratory of Materials Physics, Institute of Solid State Physics, Chinese Academy of Sciences, Hefei 230031, China

²University of Science and Technology of China, Hefei 230026, China

³Center for High Pressure Science and Technology Advanced Research, Shanghai 201203, China

⁴State Key Laboratory of High Performance Ceramics and Superfine Microstructures, Shanghai Institute of Ceramics, Chinese Academy of Sciences, Shanghai 200050, China

⁵University of Chinese Academy of Sciences, Beijing 100049, China

⁶Key Laboratory of Photochemistry, Institute of Chemistry, Chinese Academy of Sciences, Beijing 100080, China

(Received 28 May 2018; accepted 29 June 2018; published online 13 July 2018)

Recent advances in the study of thermoelectric materials mainly focus on the developments or designs of methods to reduce thermal conductivities. The information of phonon scattering processes is the key to the understanding of the thermal transfer and transport of a material. Such information is essential for the understanding of the thermal conductivity of a material itself and for the further improvement to demand the requirements for technological applications. Recently, palladium sulfide has been examined as a potential thermoelectric material. However, the high thermal conductivity limits its thermoelectric performance and technological applications. Here, Raman scattering spectroscopy is used to investigate the thermal transport properties of this material over a wide range of temperatures. The nonlinear temperature-dependent frequencies and linewidths of the Raman modes illustrate the anharmonicity of phonon scattering for thermal transport in this material. Three-phonon scattering processes are found to account for the thermal transport in the temperature range of 10–620 K. The high-energy bands of the B_g mode related to the light atom (S) contribute most to the thermal transport properties. More phonon scattering processes including higher orders are seemingly needed to further reduce the thermal conductivity of this material. *Published by AIP Publishing.* <https://doi.org/10.1063/1.5041973>

High performance thermoelectric materials have been explored for many years, to meet the urgent demand for green energy resources. The efficiency of thermoelectric materials is determined by the dimensionless figure of merit zT ($zT = S^2\sigma T/\kappa$), where S is the Seebeck coefficient, σ is the electrical conductivity, T is the absolute temperature, and κ is the thermal conductivity.^{1–5} Recently, the thermoelectric sulfides have attracted significant research interest because of their extraordinary thermoelectric performance and the cheaper and earth abundant element of sulfide.^{6,7} For instance, the copper sulfide shows high efficiency with $zTs = 1.4–1.7$ at 1000 K.⁸ Lead sulfide, which is the least studied among lead chalcogenides, shares good thermoelectric performance with $zT \sim 1$ at 1000 K.⁹ Some other materials like MS ($M = \text{Bi, Sn, Zn, and Ca}$) also share efficient thermoelectric performance.^{10–12} Palladium sulfide (PdS), which belongs to transition-metal sulfide, has potential applications in semiconducting, photoelectrochemical, and photovoltaic fields, because of its ideal bandgap of 1.6 eV.^{13–15} Moreover, superconductivity was also observed in bulk PdS by the application of pressure.¹⁶ Very recently, it was found that the bulk PdS is a promising potential thermoelectric material with an intrinsic largest power factor of $27 \mu\text{W cm}^{-1} \text{K}^{-2}$ around 800 K among thermoelectric sulfides.¹⁷ However, the

relatively high thermal conductivity limits its thermoelectric performance, even though the thermal conductivity has an obvious decrease under pressure.¹⁸ Therefore, finding the reasons behind the high thermal conductivity in this material is of great concern.

Generally speaking, κ of a normal crystal compound always has a universal behavior as a function of temperature.^{19,20} In detail, κ first increases sharply as T^3 with increasing temperature at lower temperatures and then decreases as T^{-1} or faster with increasing temperature after evolving through a maximum value at $\approx 0.05\theta_D$, where θ_D is the Debye temperature of the crystal. The high-temperature behavior of κ is mainly determined by the phonon scattering via umklapp processes.²¹ Thus, it is necessary to understand the anharmonic phonon-phonon interactions and further uncover the mechanisms of phonon scattering in candidate thermoelectrics for designing materials with low κ . Raman scattering is a powerful technique to characterize the phonon information near the center of the Brillouin zone. From the Raman spectrum, one can not only obtain the phonon dispersion near the Brillouin zone but also evaluate the phonon anharmonicity which determines the lattice thermal conductivity (κ_{lat}), especially at high temperatures.²² In detail, the anharmonicity of the phonon-phonon interactions can be reflected by the frequency shift or the variation of the full width at half maximum (FWHM) with temperature of the

^{a)}Electronic mail: xjchen@hpstar.ac.cn

Raman mode.^{23–25} However, no detailed analysis of the temperature dependent phonon information for PdS was performed until now, especially at high temperatures. Hence, it is important to analyze the phonon scattering mechanisms related to the thermal conductivity of PdS by Raman spectra. This is the goal of the present work.

The sample synthesis was detailed previously.¹⁷ For the Raman system, the scattered light with a wavelength of 488 nm was focused on 1800 g/mm grating and then recorded with a 1024 pixel Princeton charge-coupled device. The laser power of 2 mW was used in order to avoid unintentional additional heating of the sample. The obtained Raman spectra were fitted by using a Lorentzian shape function.²⁶ For the high temperature system, we used a modified diamond anvil cell (DAC) with a large anvil culet of 1000 μm in diameter. Two separated resistance heating furnaces were fixed around the two diamonds in the cell, which could supply a uniform temperature for the sample chamber. The uniform temperature around the sample chamber was measured by a kind of *K*-type thermocouple with a typical precision of ± 1 K. The high temperature range is 300–600 K with 10 K steps. The sample chamber with the diameter of 500 μm was created in a gasket (T301). A small piece of the sample (about $50 \times 50 \times 20 \mu\text{m}^3$) was loaded into the sample chamber. Then, the chamber was closed after loading protecting gas (97% argon + 3% hydrogen). For the low temperature system (10–300 K), a helium continuous flowing cryostat was used to control temperatures with 10 K steps. The temperature in the cryostat was measured by using a Pt resistance sensor close to the sample with a typical precision of ± 0.5 K. The size of the sample was about $30 \times 30 \times 20 \mu\text{m}^3$ in the sample chamber.

The crystal structure of PdS is the tetragonal structure belonging to the space group of *P42/m* (84) with unit cell parameters as follows: $a = 6.44 \pm 0.005 \text{ \AA}$ and $c = 6.62 \pm 0.005 \text{ \AA}$.¹⁷ This group has 48 optical modes by theory prediction. Among them, 21 modes are Raman active ($6B_g + 5A_g + 10E_g$), 19 modes are IR active ($14E_u + 5A_u$), and 8 modes are inactive ($2E_u + 1A_u + 5B_u$). Figure 1(c) shows the temperature dependent thermal conductivity of PdS. It can be seen that κ first increases sharply with increasing

temperature and then evolves through a maximum value before finally decreasing roughly in a T^{-1} relation. This phenomenon indicates that bulk PdS is a normal crystal compound. The emergency of the κ peak at low temperatures is caused by the approximate order between the phonon mean free path and the dimensions of the crystallite size.²⁷ Here, the thermal conductivity from the electronic part (κ_{ele}) can be ignored, because of the high lattice thermal conductivity.¹⁷ The high-temperature behavior of κ_{lat} is mainly controlled by the scattering of phonons amongst themselves for a normal crystal compound.²⁰ Generally, these phonon scattering processes can be described well by the three-phonon and/or four-phonon scattering mechanisms.^{21,28} Figure 1(b) illustrates the schematic diagrams of both three-phonon and four-phonon scattering processes, respectively. In order to provide a further understanding about the evolution of κ_{lat} at high temperatures, we now take a closer look at the phonon scattering processes with the help of the temperature-dependent Raman spectra in the temperature range of 10–620 K.

Figure 2 shows the experimentally observed Raman spectra of PdS at room temperature (lower panel) and various temperatures from 10 to 620 K (upper panel). The observed phonon modes have been assigned through theoretical calculations. We can only observe five B_g modes, three A_g modes, and one E_g mode with the excited laser wavelength of 488 nm, experimentally. This material displays strong temperature dependent Raman scattering characteristics. The frequencies of all the observed Raman bands have progressive downshifts, and the linewidths become broadened with increasing temperature from 10 to 620 K. These temperature dependent behaviors can be attributed to the anharmonic terms in the vibrational potential energy.²⁹ In addition, the spectrum exhibits two pronounced bands related to the low-energy phonons (~ 80 – 160 cm^{-1}) and high-energy phonons (~ 300 – 400 cm^{-1}). Here, the two bands are primarily caused by the vibrations of the heavy atom (Pd) and the light atom (S), respectively.^{30,31} The two phonons of the A_g mode around 134 cm^{-1} and the B_g mode around 334 cm^{-1} are selected as examples to analyze the phonon scattering processes due to their relatively good peak shapes and intensities. The A_g and B_g bands are fitted with a

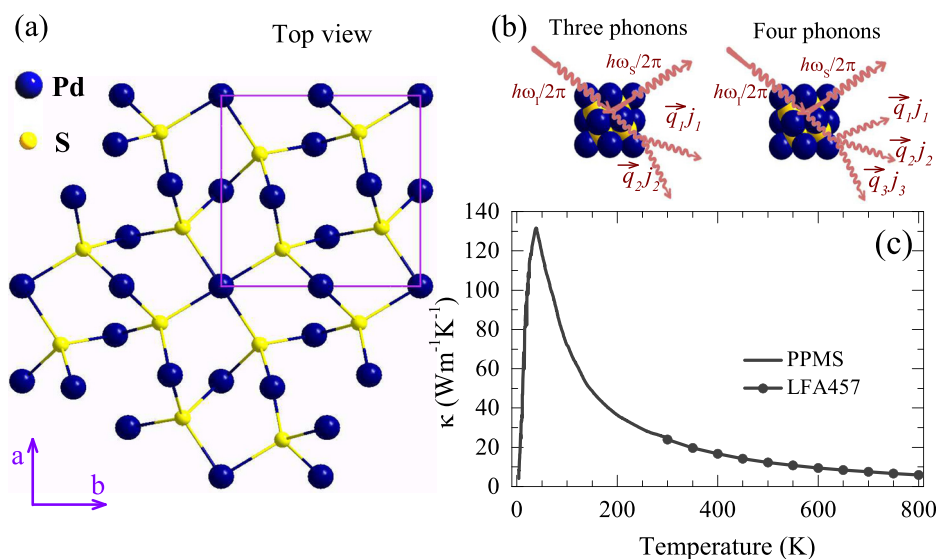


FIG. 1. (a) The crystal structure of PdS from the top view (along the *c* axis). (b) The illustrations of the three-phonon and the four-phonon anharmonic processes contributing to the decay of the Raman active modes. (c) The temperature dependence of the thermal conductivity measured by a Physical Properties Measurement System (PPMS) and a laser flash method (Netzsch, LFA 457).

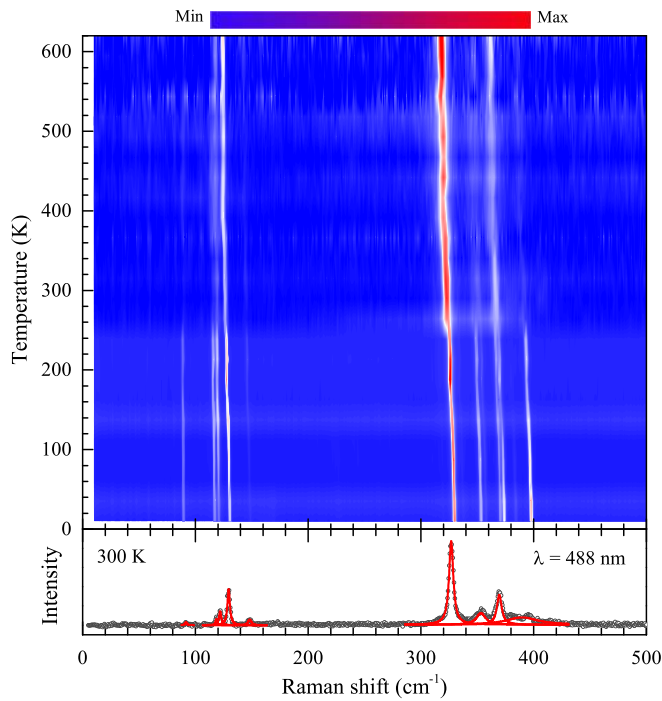


FIG. 2. Raman spectra of PdS at various temperatures from 10 to 620 K (upper panel). The lower panel shows the Raman spectrum at room temperature. The open circles are the experimental data points and the curves are the fitting results by using a single Lorentzian function for each mode.

single Lorentzian function to extract the frequencies and FWHMs.²⁶ The results are fitted very well. A representative fitted curve at room temperature can be seen in Fig. 2 (lower panel).

Based on the fitted results of the A_g mode as shown in Fig. 3(a), we present the temperature dependences of the frequency and FWHM in Figs. 3(b) and 3(c), respectively. The

evolution of both the frequency and FWHM of this phonon mode with temperature is similar to the behaviors of Si and other semiconductors.^{15,21,32} To give a reasonable description for the temperature dependence of the phonon mode position, we applied the approach based on the extended Klemens-Hart-Aggarwal-Lax model.^{33,34} In this model, the temperature-dependent Raman mode can be characterized by the processes of optical phonon decay into two (three phonon process) and/or three (four phonon process) acoustic phonons [Fig. 1(b)]. This phenomenon results from the cubic and/or quartic anharmonicity of lattice potential. Thus, the temperature dependence of the phonon mode position can be described with the following formula:³⁵

$$\omega(T) = \omega_0 + A \left[1 + \frac{2}{e^x - 1} \right] + B \left[1 + \frac{3}{e^y - 1} + \frac{3}{(e^y - 1)^2} \right], \quad (1)$$

where $x = \hbar\omega_0/2k_B T$, $y = \hbar\omega_0/3k_B T$, $\hbar\omega_0$ is the energy of optical phonon extrapolated to $T = 0$ K, \hbar is the Planck constant divided 2π , k_B is the Boltzmann constant, and A and B are the anharmonic constants. In the procedure of describing the evolution of frequency shift with temperature, we found that the three phonon process is more appropriate for this description, and the contribution from four-phonon scattering can be neglected in the studied temperature range. The four-phonon scattering may play a part at higher temperatures (at least above 620 K). The values of the fitting parameters are listed in Table I.

As shown in Fig. 3(c), the FWHM of the A_g mode around 134 cm^{-1} gets broadened with increasing temperature. The FWHM of the A_g mode has an obvious change with increasing temperature. It exhibits a nonlinear temperature

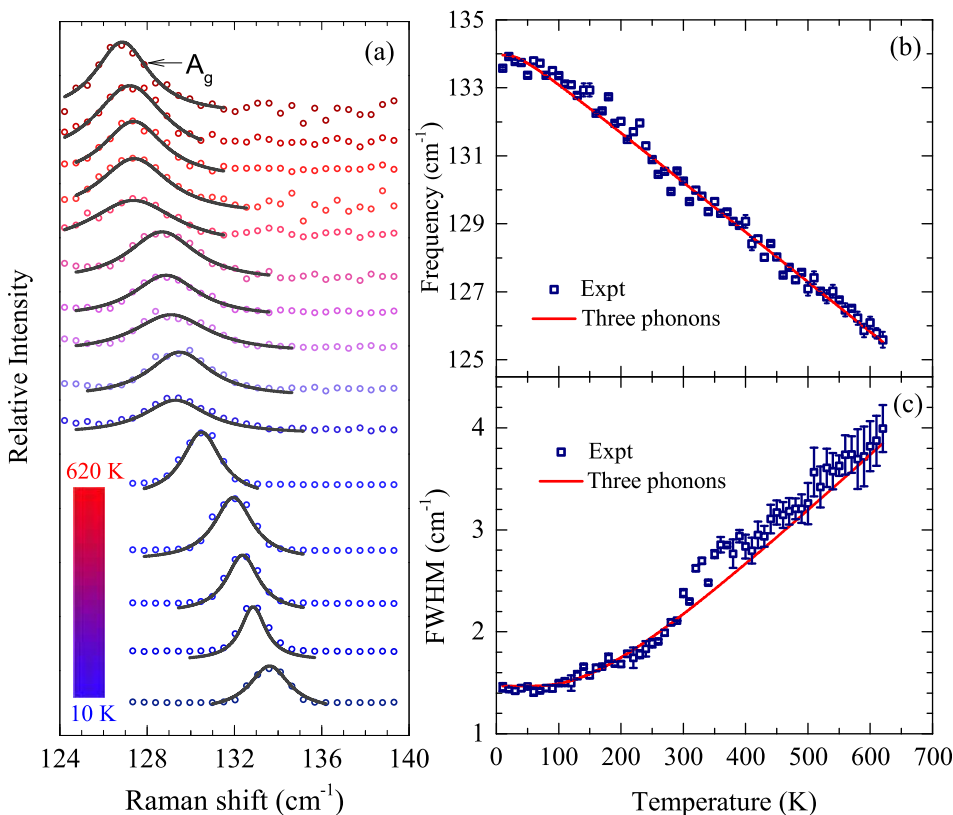


FIG. 3. (a) Raman spectra of the A_g mode around 134 cm^{-1} at various temperatures from 10 to 620 K. The open circles are the experimental data points and the curves are the fitting results by using a single Lorentzian function for the mode. Right panels: The temperature dependence of the frequency (b) and FWHM (c) of the A_g mode. The red-solid lines give the theoretical fits by using the processes of three phonon scattering.

TABLE I. Summary of the calculated phonon scattering parameters of PdS from the fits by using Eqs. (1) and (2) to the temperature dependence of the frequencies and FWHMs of the A_g and B_g modes, respectively.

Mode	ω_0 (cm $^{-1}$)	A (cm $^{-1}$)	B (cm $^{-1}$)	Γ_0 (cm $^{-1}$)	C (cm $^{-1}$)	D (cm $^{-1}$)
A_g	134.6	-0.71	0	1.4	1.37	0
B_g	333.7	-3.45	0	1.7	3.62	0

dependence. This evolution of the FWHM with temperature can be fitted according to the following equation:

$$\Gamma(T) = \Gamma_0 + C \left[1 + \frac{2}{e^x - 1} \right] + D \left[1 + \frac{3}{e^y - 1} + \frac{3}{(e^y - 1)^2} \right], \quad (2)$$

where Γ_0 is the peak width at zero temperature, and C and D are the anharmonic constants. Similar to the peak position, the FWHM curve also matches very well with the three phonon process, and the contribution from four-phonon scattering can be ignored. The fitted parameters are shown in Table I. These results indicate that the anharmonic phonon-phonon interactions (three phonon process) are responsible for the temperature dependence of the A_g mode and thus for the reduction of κ_{lat} . In addition, the phonon lifetime (τ_i), which has a close and direct correlation with κ_{lat} , is reciprocal of the FWHM of the phonon mode according to the following expression:³⁶

$$\tau_i = \frac{1}{2\pi FWHM_i}.$$

Thus, the increased FWHM of the A_g mode provides a further understanding for the decrease in κ_{lat} at high temperatures as observed in Fig. 1(c).

Figure 4 plots the temperature dependence of the B_g mode around 334 cm $^{-1}$. Both the frequency and FWHM of the B_g mode have strong temperature-dependent characteristics. Similar to the evolution of the A_g mode around 134 cm $^{-1}$, the temperature dependence of the frequency and FWHM of the B_g mode can be described well with the three phonon process. Adding the four phonon process does not improve the fitting to the experimental data. We thus do not include it in the data analysis for the simplicity. The fitted parameters are shown in Table I. Compared with the A_g mode, the B_g mode has relatively large values of A and C. This case indicates that the B_g mode has stronger anharmonic phonon-phonon interactions and thus plays a more important role in the procedure of decreasing κ_{lat} . At the same time, this conclusion is also confirmed by the phenomenon that the FWHM of the B_g mode has a larger change with temperature than that of the A_g mode. The information extracted from the B_g mode further supports the viewpoint that the three phonon process is the main player for the anharmonicity of phonon scattering in this material. Furthermore, the studied B_g mode is located at high-energy bands (~ 300 – 400 cm $^{-1}$) which is related to the vibrations of the light atom of S. This means that the vibrations of S are crucial for the thermal transport properties of PdS.

From the experimental data and theoretical models for both the A_g and B_g modes, we note that the phonons located at high-energy bands are mainly responsible for the reduction of κ_{lat} with increasing temperature. This process is realized by the process of optical phonon decay into two acoustic phonons. But the four-phonon processes which may be more important for decreasing κ_{lat} are not observed. Therefore, the enhancement of phonon anharmonicity becomes very important and useful for decreasing the thermal conductivity, such

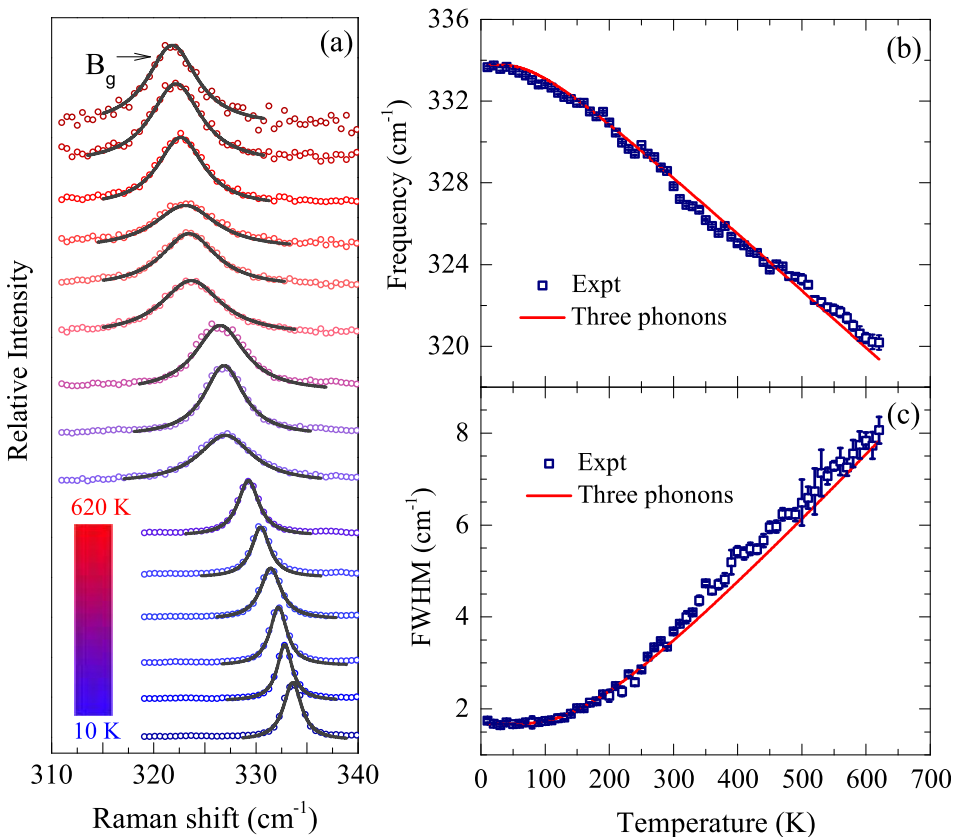


FIG. 4. (a) Raman spectra of the B_g mode around 334 cm $^{-1}$ at various temperatures from 10 to 620 K. The open circles are the experimental data points and the curves are the fitting results by using a single Lorentzian function for the mode. Right panels: The temperature dependence of the frequency (b) and FWHM (c) of the B_g mode. The red-solid lines give the theoretical fits by using the processes of three phonon scattering.

as introducing more anharmonic terms (four-phonon scattering). Many methods have been proposed to reduce thermal conductivity, such as doping, alloying, nanostructuring, and all-scale structures.^{37–40} Furthermore, we find that applying pressure is very effective in tuning the thermal conductivity by increasing the phonon anharmonicity.^{18,27}

Finally, we can conclude that the nonlinear temperature dependent frequencies and FWHMs are explained well by the phenomenon of optical phonon decay into two acoustic phonons. This case illustrated that the evolution of κ_{lat} at high temperatures is dominated by the softening and/or broadening phonon modes and thus the three-phonon processes. The results obtained in this work bring better understanding for the temperature-dependent lattice thermal conductivity. This work will further promise the process of reducing thermal conductivity for the thermoelectric PdS by introducing the stronger anharmonicity of phonon scattering.

Lei Su acknowledges the support from the National Natural Science Foundation of China (No. 21273206). Xun Shi and Li-Dong Chen acknowledge the support from the National Natural Science Foundation of China under the No. 51625205, the Key Research Program of Chinese Academy of Sciences (Grant No. KFZD-SW-421), and the Program of Shanghai Subject Chief Scientist (16XD1403900).

¹G. Chen, M. S. Dresselhaus, G. Dresselhaus, J. P. Fleurial, and T. Cailla, "Recent developments in thermoelectric materials," *Int. Mater. Rev.* **48**, 45 (2003).
²G. J. Snyder and E. S. Toberer, "Complex thermoelectric materials," *Nat. Mater.* **7**, 105 (2008).
³L. E. Bell, "Cooling, heating, generating power, and recovering waste heat with thermoelectric systems," *Science* **321**, 1457 (2008).
⁴X. Shi, L. D. Chen, and C. Uher, "Recent advances in high-performance bulk thermoelectric materials," *Int. Mater. Rev.* **61**, 379 (2016).
⁵Z. F. Ren, Y. C. Lan, and Q. Y. Zhang, *Advanced Thermoelectrics: Materials, Contacts, Devices, and Systems* (CRC Press, 2017).
⁶X. Lu, D. T. Morelli, Y. Xia, F. Zhou, V. Ozolins, H. Chi, X. Y. Zhou, and C. Uher, "High performance thermoelectricity in earth-abundant compounds based on natural mineral tetrahedrites," *Adv. Energy Mater.* **3**, 342 (2013).
⁷C. Wan, Y. Wang, N. Wang, W. Norimatsu, M. Kusunoki, and K. Koumoto, "Development of novel thermoelectric materials by reduction of lattice thermal conductivity," *Sci. Technol. Adv. Mater.* **11**, 044306 (2010).
⁸Y. He, T. Day, T. Zhang, H. Liu, X. Shi, L. D. Chen, and G. J. Snyder, "High thermoelectric performance in non-toxic earth-abundant copper sulfide," *Adv. Mater.* **26**, 3974 (2014).
⁹L. D. Zhao, S. H. Lo, J. He, H. Li, K. Biswas, J. Androulakis, C. I. Wu, T. P. Hogan, D. Y. Chung, and V. P. Dravid, "High performance thermoelectrics from earth-abundant materials: Enhanced figure of merit in PbS by second phase nanostructures," *J. Am. Chem. Soc.* **133**, 20476 (2011).
¹⁰L. D. Zhao, B. P. Zhang, W. S. Liu, H. L. Zhang, and J. F. Li, "Enhanced thermoelectric properties of bismuth sulfide polycrystals prepared by mechanical alloying and spark plasma sintering," *J. Solid State Chem.* **181**, 3278 (2008).
¹¹Q. Tan, L. D. Zhao, J. F. Li, C. F. Wu, T. R. Wei, Z. B. Xing, and M. G. Kanatzidis, "Thermoelectrics with earth abundant elements: Low thermal conductivity and high thermopower in doped SnS," *J. Mater. Chem. A* **2**, 17302 (2014).
¹²L. D. Zhao, J. He, S. Hao, C. I. Wu, T. P. Hogan, C. Wolverton, V. P. Dravid, and M. G. Kanatzidis, "Raising the thermoelectric performance of p-type PbS with endotaxial nanostructuring and valence band offset engineering using CdS and ZnS," *J. Am. Chem. Soc.* **134**, 16327 (2012).
¹³J. C. W. Folmer, J. A. Turner, and B. A. Parkinson, "Photoelectrochemical characterization of several semiconducting compounds of palladium with sulfur and/or phosphorus," *J. Solid State Chem.* **68**, 28 (1987).

¹⁴I. J. Ferrer, P. D. Chao, A. Pascual, and C. Sánchez, "An investigation on palladium sulphide (PbS) thin films as a photovoltaic material," *Thin Solid Films* **515**, 5783 (2007).
¹⁵M. Barawi, I. J. Ferrer, J. R. Ares, and C. Sánchez, "Hydrogen evolution using palladium sulfide (PbS) nanocrystals as photoanodes in aqueous solution," *ACS Appl. Mater. Interfaces* **6**, 20544 (2014).
¹⁶L. C. Chen, H. Yu, H. J. Pang, B. B. Jiang, L. Su, X. Shi, L. D. Chen, and X. J. Chen, "Pressure-induced superconductivity in palladium sulfide," *J. Phys.: Condens. Matter* **30**, 155703 (2018).
¹⁷L. C. Chen, B. B. Jiang, H. Yu, H. J. Pang, L. Su, X. Shi, L. D. Chen, and X. J. Chen, "Thermoelectric properties of polycrystalline material palladium sulfide," *RSC Adv.* **8**, 13154 (2018).
¹⁸L. C. Chen, H. Yu, H. J. Pang, B. B. Jiang, L. Su, X. Shi, L. D. Chen, and X. J. Chen, "Pressure-induced enhancement of thermoelectric performance in palladium sulfide," *Mater. Today Phys.* **5**, 64 (2018).
¹⁹J. Callaway, "Model for lattice thermal conductivity at low temperatures," *Phys. Rev.* **113**, 1046 (1959).
²⁰D. T. Morelli and J. P. Heremans, "Estimation of the isotope effect on the lattice thermal conductivity of group IV and group III–V semiconductors," *Phys. Rev. B* **66**, 195304 (2002).
²¹T. L. Feng and X. L. Ruan, "Quantum mechanical prediction of four-phonon scattering rates and reduced thermal conductivity of solids," *Phys. Rev. B* **93**, 045202 (2016).
²²E. S. Toberer, L. L. Baranowski, and C. Dames, "Advances in thermal conductivity," *Annu. Rev. Mater. Res.* **42**, 179 (2012).
²³Z. D. Mitrović, Z. V. Popović, and M. Šćepanović, "Anharmonicity effects in nanocrystals studied by Raman scattering spectroscopy," *Acta Phys. Pol. B* **116**, 36 (2009).
²⁴R. Cuscó, E. Alarcón-Lladó, J. Ibáñez, L. Artús, J. Jiménez, B. G. Wang, and M. J. Callahan, "Temperature dependence of Raman scattering in ZnO," *Phys. Rev. B* **75**, 165202 (2007).
²⁵N. Domènech-Amador, R. Cuscó, L. Artús, T. Yamaguchi, and Y. Nanishi, "Raman scattering study of anharmonic phonon decay in InN," *Phys. Rev. B* **83**, 245203 (2011).
²⁶R. K. Singh, S. N. Singh, B. P. Asthana, and C. M. Pathak, "Deconvolution of Lorentzian Raman linewidth: Techniques of polynomial fitting and extrapolation," *J. Raman Spectrosc.* **25**, 423 (1994).
²⁷H. Yu, L. C. Chen, H. J. Pang, X. Y. Qin, P. F. Qiu, X. Shi, L. D. Chen, and X. J. Chen, "Impressive enhancement of thermoelectric performance in CuInTe₂ upon compression," *Mater. Today Phys.* **5**, 1 (2018).
²⁸L. Lindsay and D. A. Broido, "Three-phonon phase space and lattice thermal conductivity in semiconductors," *J. Phys.: Condens. Matter* **20**, 165209 (2008).
²⁹I. P. Ipatova, A. A. Maradudin, and R. F. Wallis, "Temperature dependence of the width of the fundamental lattice-vibration absorption peak in ionic crystals. II. approximate numerical results," *Phys. Rev.* **155**, 882 (1967).
³⁰X. J. Chen, V. V. Struzhkin, S. Kung, H. K. Mao, R. J. Hemley, and A. N. Christensen, "Pressure-induced phonon frequency shifts in transition-metal nitrides," *Phys. Rev. B* **70**, 014501 (2004).
³¹D. Bansal, J. W. Hong, C. W. Li, A. F. May, W. Porter, M. Y. Hu, D. L. Abernathy, and O. Delaire, "Phonon anharmonicity and negative thermal expansion in SnSe," *Phys. Rev. B* **94**, 054307 (2016).
³²A. Taube, J. Judek, C. Jastrzębski, A. Duzynska, K. Switkowski, and M. Zdrojek, "Temperature-dependent nonlinear phonon shifts in a supported MoS₂ monolayer," *ACS Appl. Mater. Interfaces* **6**, 8959 (2014).
³³P. G. Klemens, "Anharmonic decay of optical phonons," *Phys. Rev.* **148**, 845 (1966).
³⁴T. R. Hart, R. L. Aggarwal, and B. Lax, "Temperature dependence of Raman scattering in silicon," *Phys. Rev. B* **1**, 638 (1970).
³⁵M. Balkanski, R. F. Wallis, and E. Haro, "Anharmonic effects in light scattering due to optical phonons in silicon," *Phys. Rev. B* **28**, 1928 (1983).
³⁶A. M. Hofmeister, "Pressure dependence of thermal transport properties," *Proc. Natl. Acad. Sci. U. S. A.* **104**, 9192 (2007).
³⁷B. C. Sales, D. Mandrus, and R. K. Williams, "Filled skutterudite antimonides: A new class of thermoelectric materials," *Science* **272**, 1325 (1996).
³⁸L. P. Hu, T. J. Zhu, X. H. Liu, and X. B. Zhao, "Point defect engineering of high-performance bismuth-telluride-based thermoelectric materials," *Adv. Funct. Mater.* **24**, 5211 (2014).
³⁹J. P. Heremans, V. Jovovic, E. S. Toberer, A. Saramat, K. Kurosaki, A. Charoenphakdee, S. Yamanaka, and G. J. Snyder, "Enhancement of thermoelectric efficiency in PbTe by distortion of the electronic density of states," *Science* **321**, 554 (2008).
⁴⁰K. Biswas, J. He, I. D. Blum, C. I. Wu, T. P. Hogan, D. N. Seidman, V. P. Dravid, and M. G. Kanatzidis, "High-performance bulk thermoelectrics with all-scale hierarchical architectures," *Nature (London)* **489**, 414 (2012).